DRAFT VERSION AUGUST 4, 2014
Preprint typeset using LaTeX style emulateapj v. 5/2/11

arXiv:1407.0348v2 [astro-ph.HE] 31 Jul 2014

MULTI-WAVELENGTH AFTERGLOWS OF FAST RADIO BURSTS

SHUANG-XI YI[1], HE GAO, BING ZHANG
Department of Physics and Astronomy, University of Nevada Las Vegas, NV 89154, USA; zhang@physics.unlv.edu
Draft version August 4, 2014

ABSTRACT

The physical nature of fast radio bursts (FRBs) is not identified. Detecting electromagnetic counterparts in other wavelengths is essential to measure their distances and to settle down their physical nature. Assuming that at least some of them are of a cosmological origin, we calculate their afterglow lightcurves in multi-wavelengths (X-rays, optical and radio) by assuming a range of their total kinetic energies and redshifts. We focus on forward shock emission, but also consider the possibility that some of them might have bright reverse shock emission. In general, the FRB afterglows are too faint to be detected by current detectors. Only if an FRB has a very low radiative efficiency in radio (hence, a very large kinetic energy), and when it is close enough, can its afterglow be detected in the optical and radio bands. We discuss observational strategies to detect these faint afterglows using future telescopes such as LSST and EVLA.

Subject headings: gamma ray: bursts — radiation mechanism: non-thermal

1. INTRODUCTION

Fast radio bursts (FRBs) are mysterious transients discovered recently (Lorimer et al. 2007; Thornton et al. 2013). Their physical origin is subject to intense debate (e.g. Falcke & Rezzolla 2014; Totani 2013; Kashiyama et al. 2013; Popov & Postnov 2013; Zhang 2014; Loeb et al. 2014; Kulkarni et al. 2014). If at least some FRBs are of a cosmological origin, as indicated by the anomolously large dispersion measure (DM), their redshift information together with the measured DM offer a powerful tool to study cosmology, including inferring the baryon content and reionization history of the universe (Deng & Zhang 2014; Kulkarni et al. 2014), and directly constraining cosmological parameters and dark matter equation of state (Gao et al. 2014; Zhou et al. 2014).

The error boxes of FRBs detected by Parkes multi-beam survey are typically hundreds of square arc-minutes (Thornton et al. 2013). It is therefore difficult to pin down their host galaxies and derive their redshifts. Detecting counterparts of FRBs in other wavelengths would be essential to localize FRBs. Kashiyama et al. (2013) suggested binary white dwarf (WD) mergers as the source of FRBs, and proposed possible associations of some FRBs with Type Ia SNe or X-ray debris disk emission. Motivated by Swift data showing evidence of a supra-massive neutron star collapsing into a black hole (Troja et al. 2007; Lyons et al. 2010; Rowlinson et al. 2010, 2013; Lü & Zhang 2014; Yi et al. 2014), Zhang (2014) suggested possible associations of a small fraction of FRBs with GRBs. Two tentative associations of FRB-like events with GRBs may have been discovered by Bannister et al. (2012)[2]. Unfortunately, the redshifts of the two GRBs were not measured.

Another possibility is to search for the afterglow of FRBs. Zhang (2014) estimated the brightness of FRB afterglows, and found that it is very faint owing to their low energetics. He suggested that for a typical FRB at a cosmological distance, the peak radio afterglow flux is dimmer than the FRB itself by 6-7 orders of magnitude (at the μJy level). In this paper, we calculate the multi-wavelength FRB afterglows in detail.

[1] School of Astronomy and Space Science, Nanjing University, Nanjing 210093

[2] A negative search result was reported by Palaniswamy et al. (2014), but the time windows of some of these GRBs did not cover the end of the plateau, which is the expected epoch of FRB emission (Zhang 2014).

2. THE MODEL

We apply the standard external shock synchrotron emission afterglow model of GRBs (Mészáros & Rees 1997; Sari et al. 1998; see Gao et al. 2013a for a recent, detailed review). The simplest afterglow model has several free parameters: the total kinetic energy E, the initial Lorentz factor η, the number density of the ambient medium n_0; the equipartition parameters ε_e, ε_B for electrons and magnetic fields, respectively; and the electron injection spectral index p. If one considers a pair of (forward and reverse) shocks, the micro-physics parameters can be different for the two shocks. So altogether one has nine parameters.

The forward shock (FS) emission component is guaranteed. Whether a bright reverse shock (RS) emission component exists depends on the unknown magnetization parameter (the ratio between Poynting flux and matter flux, usually denoted as σ) of the outflow (Zhang & Kobayashi 2005; Mimica et al. 2009; Mizuno et al. 2009). Most FRB models invoke highly magnetized neutron stars or black holes (e.g. Falcke & Rezzola 2014; Totani 2013; Zhang 2014; Popov & Postnov 2013). For example, in the "magnetic hair" ejection model invoking the implosion of a supra-massive neutron star (Falcke & Rezzola 2014; Zhang 2014), an FRB is emitted in the ejected magnetosphere. The outflow is therefore likely highly magnetized at the central engine. The outflow is accelerated via a magnetic pressure gradient (e.g. Komissarov et al. 2009; Granot et al. 2011), so that σ decreases with radius with the expense of increasing Γ. Significant magnetic dissipation would also occur during the FRB emission phase. Therefore the σ value after the dissipation, especially at the deceleration radius, is not known. If it is already below unity, as envisaged in some models (e.g. Zhang & Yan 2011), a bright reverse shock emission component may be expected (Zhang et al. 2003; Zhang & Kobayashi 2005).

In the following we neglect these complications, and only consider a standard fireball defined by the total energy E and initial Lorentz factor η. For faint afterglows of FRBs, to the first order the details of jet composision would not affect the global picture.

The deceleration time scale $t_\times$, which is also the time when

the reverse shock crosses the shell (for a non-magnetized outflow), can be approximated as

$$t_\times \sim \frac{l(1+z)}{2c\eta^{8/3}}, \quad (1)$$

where $l = (3E/4\pi n_0 m_p c^2)^{1/3}$ is the Sedov length.

Both E and η are poorly constrained. The observed FRBs have an energy $E_{\rm FRB} \sim 10^{38} - 10^{40}$ erg assuming a redshift $z \sim (0.5-1)$ (Thornton et al. 2013). Observations of radio pulsars suggest that their radio emission efficiency is typically low, especially for more energetic ones (Szary et al. 2014). As a result, the total kinetic energy in an FRB outflow can be significantly greater than the FRB energy. Within the supramassive neutron star implosion scenario, the total energy in the ejecta is essentially the total magnetic energy of the neutron star magnetosphere, which can be as large as $\sim 10^{47}$ erg for a magnetar (Zhang 2014). In the following, we allow E to be in a wide range from $10^{43} - 10^{47}$ erg.

Various constraints on the FRB emission mechanisms suggest that the bulk motion Lorentz factor of an FRB is at least 100 (e.g. Falcke & Rezzolla 2014; Katz 2014). In the following, we adopt a conservative value $\eta = 100$. At $t \gg t_\times$, the predictions of afterglow flux do not depend on η. For a higher η, $t_\times$ would move to an earlier epoch, and the peak afterglow flux would be increased accordingly. For $E = 10^{47}$ erg, $\eta = 100$, and $n_0 \sim 1$ cm^{-3}, one has $t_\times \sim 3$ s.

The synchrotron radiation spectrum from the FS or RS can be characterized by a multi-segment broken power law separated by three characteristic frequencies: the minimum synchrotron frequency (corresponding to electrons with the minimum Lorentz factor), the cooling frequency ν_c, and the self-absorption frequency ν_a (Sari et al. 1998). The peak flux of the spectrum is denoted as $F_{\nu,\rm max}$. Based on the standard prescription (e.g. Sari et al. 1998; Wu et al. 2003; Yi et al. 2013; Gao et al. 2013a), one can calculate the afterglow emission from FRBs. At the shock crossing time $t_\times$, the FS emission can be characterized by

$$\nu^f_{\rm m,\times} = 4.1\times10^{16}\varepsilon_{B,f,-2}^{1/2}\varepsilon_{e,-1}^{2} n_0^{1/2}\eta_2^4(1+z)^{-1}\,{\rm Hz}, \quad (2)$$

$$\nu^f_{c,\times} = 7.5\times10^{19}\varepsilon_{B,f,-2}^{-3/2} n_0^{-5/6}\eta_2^{4/3}E_{47}^{-2/3}(1+z)^{-1}\,{\rm Hz}, \quad (3)$$

$$\nu^f_{a,\times} = 7.4\times10^{8}\varepsilon_{B,f,-2}^{1/5}\varepsilon_{e,-1}^{-1} n_0^{3/5}E_{47}^{1/5}(1+z)^{-1}\,{\rm Hz}, \quad (4)$$

$$F^f_{\nu,\rm max,\times} = 7.8\times10^{-6}\varepsilon_{B,f,-2}^{1/2} n_0^{1/2}E_{47}D_{L,27}^{-2}(1+z)\,{\rm Jy}. \quad (5)$$

Here the typcial shock micro-physics parameters are normalized to $\varepsilon_e = 0.1$, $\varepsilon_B = 0.01$, and $p = 2.5$. The evolution of the four parameters (Mészáros & Rees 1997; Sari et al. 1998; Yi et al. 2013; Gao et al. 2013a)

$$t<t_\times:\ \nu_a^f\propto t^{\frac{3}{5}}, \nu_m^f\propto t^0, \nu_c^f\propto t^{-2}, F^f_{\nu,\rm max}\propto t^3, \quad (6)$$

and

$$t>t_\times:\ \nu_a^f\propto t^0, \nu_m^f\propto t^{-\frac{3}{2}}, \nu_c^f\propto t^{-\frac{1}{2}}, F^f_{\nu,\rm max}\propto t^0. \quad (7)$$

Because of a small total energy, an FRB outflow would reach the non-relativistic phase in a relatively short period of time. The transition time is when the bulk Lorentz factor $\gamma - 1 = 1$, where $\gamma \sim (3E/32\pi n_0 m_p c^5 t^3)^{1/8}$. After this transition time, the scaling law of the FS emission is modified as

$$\nu_a^f\propto t^{\frac{6}{5}}, \nu_m^f\propto t^{-3}, \nu_c^f\propto t^{-\frac{1}{5}}, F^f_{\nu,\rm max}\propto t^{\frac{3}{5}}. \quad (8)$$

The non-relativistic phase transition time is roughly $t_{\rm N} \sim 6.6\times10^4, 1.4\times10^4, 3.1\times10^3$ s for with $E = 10^{47}, 10^{45}, 10^{43}$ erg, respectively.

If a putative RS exists, the four parameters $(\nu_m, \nu_c, \nu_a, F_{\nu,\rm max})$ of the two shocks can be related to each other at $t_\times$, which depend on the ratios between the micro-physics parameters of the two shocks (Kobayashi & Zhang 2003; Zhang et al. 2003). When explicitly written, these four parameters are

$$\nu^r_{m,\times} = 1.3\times10^{13}\varepsilon_{B,r,-1}^{1/2}\varepsilon_{e,-1}^{2} n_0^{1/2}\eta_2^2(1+z)^{-1}\,{\rm Hz}, \quad (9)$$

$$\nu^r_{c,\times} = 2.4\times10^{18}\varepsilon_{B,r,-1}^{-3/2} n_0^{-5/6}\eta_2^{4/3}E_{47}^{-2/3}(1+z)^{-1}\,{\rm Hz}, \quad (10)$$

$$\nu^r_{a,\times} = 7.2\times10^{11}\varepsilon_{B,r,-1}^{1/5}\varepsilon_{e,-1}^{-1} n_0^{3/5}\eta_2^{8/5}E_{47}^{1/5}(1+z)^{-1}{\rm Hz}, \quad (11)$$

$$F^r_{\nu,\rm max,\times} = 2.5\times10^{-3}\varepsilon_{B,r,-1}^{1/2} n_0^{1/2}\eta_2 E_{47}D_{L,27}^{-2}(1+z)\,{\rm Jy}. \quad (12)$$

Notice that ε_B is normalized to 0.1, in view that the outflow is likely magnetized.

The scaling laws of RS before and after the crossing time are (e.g. Kobayashi 2000; Yi et al. 2013; Gao et al. 2013a)

$$t<t_\times:\ \nu_a^r\propto t^{-\frac{33}{10}}, \nu_m^r\propto t^6, \nu_c^r\propto t^{-2}, F^r_{\nu,\rm max}\propto t^{\frac{3}{2}}, \quad (13)$$

and

$$t>t_\times:\ \nu_a^r\propto t^{-\frac{102}{175}}, \nu_m^r\propto t^{-\frac{54}{35}}, \nu_c^r\propto t^{-\frac{54}{35}}, F^r_{\nu,\rm max}\propto t^{-\frac{34}{35}}. \quad (14)$$

3. RESULTS

Figure 1 shows the calculated FS FRB afterglow lightcurves in the X-ray (2 keV, panel a), optical (R-band, panel b), and radio (1 GHz, panel c) bands, respectively. Three different energies, i.e. $E = 10^{47}$ erg (blue), 10^{45} erg (red), and 10^{43} erg (green), and three different redshifts, i.e. $z = 0.5$ (dashed), 0.1 (dash-dotted), and 0.01 (solid), have been adopted. Other parameters are fixed to the typical values: $\eta = 100$, $n_0 = 1$ cm^{-3}, $p = 2.5$, $\epsilon_{B,f} = 0.01$, and $\epsilon_e = 0.1$. The sensitivity lines of different detectors in different energy bands are also plotted. The black solid line in panel a is the sensitivity line of *Swift*/X-Ray Telescope (XRT), which is $\propto t^{-1}$ early on, and breaks to $\propto t^{-1/2}$ when $F_\nu = 2.0\times10^{-15}$erg cm^{-2} s^{-1} at $t = 10^5$ s (Moretti et al. 2009, D. N. Burrows, 2014, private communication). The black solid line in panel b is the sensitivity line of the Large Synoptic Survey Telescope Array (LSST). In the survey mode, LSST reaches 24.5 mag in 30 seconds (R. Margutti, 2014, private communication). The black solid line in panel c is the sensitivity line of the Expanded Very Large Array (EVLA)[3], which scales as $\propto t^{-1/2}$ for arbitrarily long exposure times.

In general, the broad-band FRB afterglows are all very faint. Only for a large E and a small z, when the predicted afterglow flux becomes of an observational interest. As shown in Figure 1, the X-ray afterglow becomes detectable by *Swift*/XRT only for the most optimistic case calculated, i.e. $E = 10^{47}$ erg, and $z = 0.01$ (panel a). In the optical R-band (panel b), the peak magnitude of the FS light curves are about 17, 22, 26, respectively, for $z = 0.01, 0.1, 0.5$ and $E = 10^{47}$ erg. The LSST may catch the peak emission only when $z < 0.2$ for $E = 10^{47}$ erg. In the 1 GHz radio band (panel c), the peak flux density are about 4.4×10^{-4} Jy, 4.2×10^{-6} Jy, and 1.5×10^{-7}

[3] The Exposure Calculator can be found at https://obs.vla.nrao.edu/ect/

Jy, respectively, for $z = 0.01, 0.1, 0.5$ and $E = 10^{47}$ erg. This would be detected by EVLA only when $z < 0.2$ for $E = 10^{47}$ erg. The peak time shifts to later times with dereasing frequency. This suggests that follow-up observations are easier in low frequencies. For example, with $E = 10^{47}$ erg, the peak time in 1 GHz is around 1 day.

We also consider the RS emission from FRBs in Figure 2. Fixing other parameters, we allow $\varepsilon_{B,r}$ to be higher than $\varepsilon_{B,f}$ in view that the outflow is likely highly magnetized. Defining $R_{\rm B} = (\varepsilon_{B,r}/\varepsilon_{B,f})^{1/2}$ (Zhang et al. 2003), we calculate the cases for $R_{\rm B} = 2$ (purple), 5 (blue), and 8 (red). We fix $E = 10^{47}$ erg and consider $z = 0.01$ and $z = 0.1$, with the FS emission (green) plotted as a reference. One can see that with a large $R_{\rm B}$, the RS component would outshine the FS component, especially in the optical and radio bands, making it easier to detect. The afterglow is detectable by LSST and EVLA at $z < 0.2$.

To better display how peak time and peak flux depend on E and z, in Figure 3 we show the contours of peak time and peak flux in the $E - z$ space. The three panels are for X-rays (panel a), optical (panel b) and radio (panel c), respectively. The X-ray peak time is simply the deceleration time $t_\times$. For the optical band, the peak time is defined when ν_m crosses the band. For the radio band, the peak time is defined when $\max(\nu_m, \nu_a)$ crosses the band. For the peak flux, we present two (FS vs. RS) values, with the RS value presented in the parenthesis (noticing the same E- and z-dependences of $F^f_{\nu,\rm max}$ and $F^r_{\nu,\rm max}$. Since the sensitivity of LSST in the survey mode is a constant (24.5 mag), we also plotted two thick lines (24.5 mag) above which LSST can detect the FS (magenta) and RS (green) emissions, respectively.

Assuming that most observed FRBs are at $z \sim 1$, one can derive the event rate for FRBs below a certain redshift. Assuming that the total event rate density is a constant, i.e. $\rho \sim 10^{-3}$ gal^{-1} yr^{-1} (Thornton et al. 2013), a smaller redshift corresponds to a small volume, and hence, a small event rate. Taking an event rate of $\sim 10^4$ sky^{-1} day^{-1} at $z \sim 1$ (Thornton et al. 2013), one can draw the expected event rate as a function of z based on volume correction. This is shown as blue dotted lines in the three contour plots. Notice that the event rate is subject to large uncertainties. For example, recently Petroff et al (2014) reported a lack of FRBs at intermediate Galactic latitudes, which suggests either a possible anisotropy of FRB distribution or a lower event rate. Our event rate curve is still relevant as long as one re-normalize the $z = 1$ event rate to whatever value determined by future observations.

4. SUMMARY AND DISCUSSION

In this paper, we apply the standard GRB afterglow model to predict possible afterglow emission from FRBs. We calculate their afterglow lightcurves in X-rays, optical, and radio by assuming a range of their total kinetic energies and redshifts. In general, owing to their low energetics, the broad-band afterglow emission is predicted to be very faint, especially for the FS only. Only if the total kinetic energy of FRBs is very large (radio efficiency very low), and in rare cases when some of them are close enough to earth, could their FS afterglows become (barely) detectable by the current instruments. It is unclear whether there is a bright RS component from FRBs. If so (which requires significant de-magnetization before deceleration), the chance of detecting FRB afterglow in the optical and radio bands is higher, even though still challenging.

Since data analyses needed to claim the detection of an FRB take significant time, and since the X-ray afterglow of an FRB peaks early and decays rapidly, follow up observations of FRBs with X-ray telescopes (e.g. Swift/XRT) would not be fruitful. A better strategy to detect an X-ray counterpart of an FRB is to apply a wide-field X-ray telescope (such as Einstein Probe and Lobster), which may catch an X-ray transient associated with an FRB. However, such a telescope is still being proposed, and it is believed that several other types X-ray transients, e.g. supernova shock breakouts (Soderberg et al. 2008), jets from tidal disruption events (Burrows et al. 2011; Bloom et al. 2011), and putative X-ray transients due to neutron star - neutron star mergers with a millisecond magnetar engine (Zhang 2013; Gao et al. 2013b; Yu et al. 2013; Metzger & Piro 2014)[4], would give rise to brighter X-ray signals than the FRB afterglow. Detecting X-ray transients associated with FRBs is plausible, but challenging.

In the optical band, the FS peak time is after $t_\times$, while the RS peak time is at $t_\times$. Again due to the possible delay of data analysis to claim an FRB discovery, follow-up observations may not be fruitful. One should also appeal to wide-field optical telescopes, such as GWAC (Paul et al. 2011). The peak flux is however usually too low to be detected by these telescopes, unless the source is energetic, nearby, and with a bright RS emission component. The optical afterglow peak emission can be detected by LSST for nearby energetic events in the survey mode. However, since only 7-10 square degrees are covered in each 30 seconds exposure (E. Berger, 2014, private communication), it still takes great chance coincidence to detect the optical afterglow of an FRB with LSST.

In the radio band, the telescope that detects the FRB can continue to collect data. As a result, no trigger information is needed to "follow-up" an FRB. On the other hand, the afterglow is faint. For a Jy-level FRB, the peak afterglow flux is in the μJy level for the FS component for typical parameters, and at most one order of magnitude brighter for the RS component. For optimistic cases (large E and small z), the afterglow flux may reach the mJy level, but the detection rate for these extreme cases is very low. In general, large radio telescopes with high sensitivity is needed. In principle, one can use a small radio telescope to trigger an FRB and use a large telescope to follow up. The peak time of radio afterglow is $10^4 - 10^6$ s (hours to days). This would be a good strategy if the data processing time to claim an FRB detection can be reduced to within hours. Follow up observations with EVLA would be able to catch the FRB afterglow if the source is energetic and nearby.

The afterglow emission signal discussed in this paper is *generic* to progenitor models. It is also the *minimum* multi-wavelength signals one would expect to be associated with an FRB. Subject to progenitor models, an FRB may be accompanied by other brighter signals (e.g. Kashiyama et al. 2013; Zhang 2014; Niino et al. 2014), which can be used to differentiate among the progenitor models.

We thank Edo Berger, David Burrows, and Raffaella Margutti for helpful discussions on the instrumental sensitivities of EVLA, LSST, and Swift XRT.

[4] Double neutron star mergers can leave behind a supra-massive rapidly spinning neutron star if the mass of the two neutron stars are small and the neutron star equation of state is hard (Dai et al. 2006; Gao & Fan 2006).

REFERENCES

Bannister, K. W., Murphy, T., Gaensler, B. M., & Reynolds, J. E. 2012, ApJ, 757, 38
Bloom, J. S., Giannios, D., Metzger, B. D., et al. 2011, Science, 333, 203
Burrows, D. N., Kennea, J. A., Ghisellini, G., et al. 2011, Nature, 476, 421
Burrows, D. N., Frank, K. A., & Park, S. 2014, American Astronomical Society Meeting Abstracts, 223, #353.14
Dai, Z. G., Wang, X. Y., Wu, X. F. & Zhang, B. 2006, Science, 311, 1127
Deng, W., & Zhang, B. 2014, ApJ, 783, L35
Falcke, H., & Rezzolla, L. 2014, A&A, 562, A137
Gao, H., Ding, X., Wu, X.-F., Zhang, B., & Dai, Z.-G. 2013b, ApJ, 771, 86
Gao, H., Lei, W.-H., Zou, Y.-C., Wu, X.-F., & Zhang, B. 2013a, New Astron. Rev., 57, 141
Gao, H., Li, Z., & Zhang, B. 2014, ApJ, 788, 189
Gao, W.-H. & Fan, Y.-Z. 2006, ChJAA, 6, 513
Granot, J., Komissarov, S. S., & Spitkovsky, A. 2011, MNRAS, 411, 1323
Kashiyama, K., Ioka, K., & Mészáros, P. 2013, ApJ, 776, L39
Katz, J. I. 2014, Phys. Rev. D, 89, 103009
Kobayashi, S. 2000, ApJ, 545, 807
Kobayashi, S., & Zhang, B. 2003, ApJ, 582, L75
Komissarov, S. S., Vlahakis, N., Königl, A., & Barkov, M. V. 2009, MNRAS, 394, 1182
Kulkarni, S. R., Ofek, E. O., Neill, J. D., Zheng, Z., & Juric, M. 2014, arXiv:1402.4766
Loeb, A., Shvartzvald, Y., & Maoz, D. 2014, MNRAS, 439, L46
Lorimer, D. R., Bailes, M., McLaughlin, M. A., Narkevic, D. J., & Crawford, F. 2007, Science, 318, 777
Lü, H.-J. & Zhang, B. 2014, ApJ, 785, 74
Lyons, N., O'Brien, P. T., Zhang, B., Willingale, R., Troja, E., & Starling, R. L. C. 2010, MNRAS, 402, 705
Mészáros, P., & Rees, M. J. 1997, ApJ, 476, 232
Metzger, B. D., & Piro, A. L. 2014, MNRAS, 439, 3916
Mimica, P., Giannios, D., & Aloy, M. A. 2009, A&A, 494, 879
Mizuno, Y., Zhang, B., Giacomazzo, B., et al. 2009, ApJ, 690, L47
Moretti, A., Pagani, C., Cusumano, G., et al. 2009, A&A, 493, 501
Niino, Y., Totani, T. & Okumura, J. E. 2014, PASJ, submitted (arXiv:1407.1088)
Palaniswamy, D., Wayth, R. B., Trott, C. M., McCallum, J. N., Tingay, S. J. & Reynolds, C. 2014, ApJ, in press, arXiv:1406.1850
Paul, J., Wei, J., Basa, S. & Zhang, S.-N. 2011, Comptes Rendus Physique, 12, 298
Petroff, E., van Straten, W., Johnston, S., et al. 2014, arXiv:1405.5945
Popov, S. B., & Postnov, K. A. 2013, arXiv:1307.4924
Rowlinson, A., O'Brien, P. T., Tanvir, N. R., Zhang, B., Evans, P. A. et al. 2010, MNRAS, 409, 531
Rowlinson, A. O'Brien, P. T., Metzger, B. D., Tanvir, N. R. & Levan, A. J. 2013, MNRAS, 430, 1061
Sari, R., Piran, T., & Narayan, R. 1998, ApJ, 497, L17
Soderberg, A. M., Berger, E., Page, K. L., et al. 2008, Nature, 453, 469
Szary, A., Zhang, B., Melikidze, G. I., Gil, J., & Xu, R.-X. 2014, ApJ, 784, 59
Thornton, D., Stappers, B., Bailes, M., et al. 2013, Science, 341, 53
Totani, T. 2013, PASJ, 65, L12
Troja, E., Cusumano, G., O'Brien, P. T., Zhang, B., Sbarufatti, B. et al. 2007, ApJ, 665, 599
Wu, X. F., Dai, Z. G., Huang, Y. F., & Lu, T. 2003, MNRAS, 342, 1131
Yi, S.-X., Wu, X.-F., & Dai, Z.-G. 2013, ApJ, 776, 120
Yi, S.-X., Dai, Z.-G., Wu, X.-F. & Wang, F. Y. 2014, arXiv:1401.1601
Yu, Y.-W., Zhang, B., & Gao, H. 2013, ApJ, 776, L40
Zhang, B. 2014, ApJ, 780, L21
Zhang, B. 2013, ApJ, 763, L22
Zhang, B., & Kobayashi, S. 2005, ApJ, 628, 315
Zhang, B., Kobayashi, S., & Mészáros, P. 2003, ApJ, 595, 950
Zhang, B. & Yan, H. 2011, ApJ, 726, 90
Zhou, B., Li, X., Wang, T., Fan, Y.-Z., & Wei, D.-M. 2014, Phys. Rev. D, 89, 107303

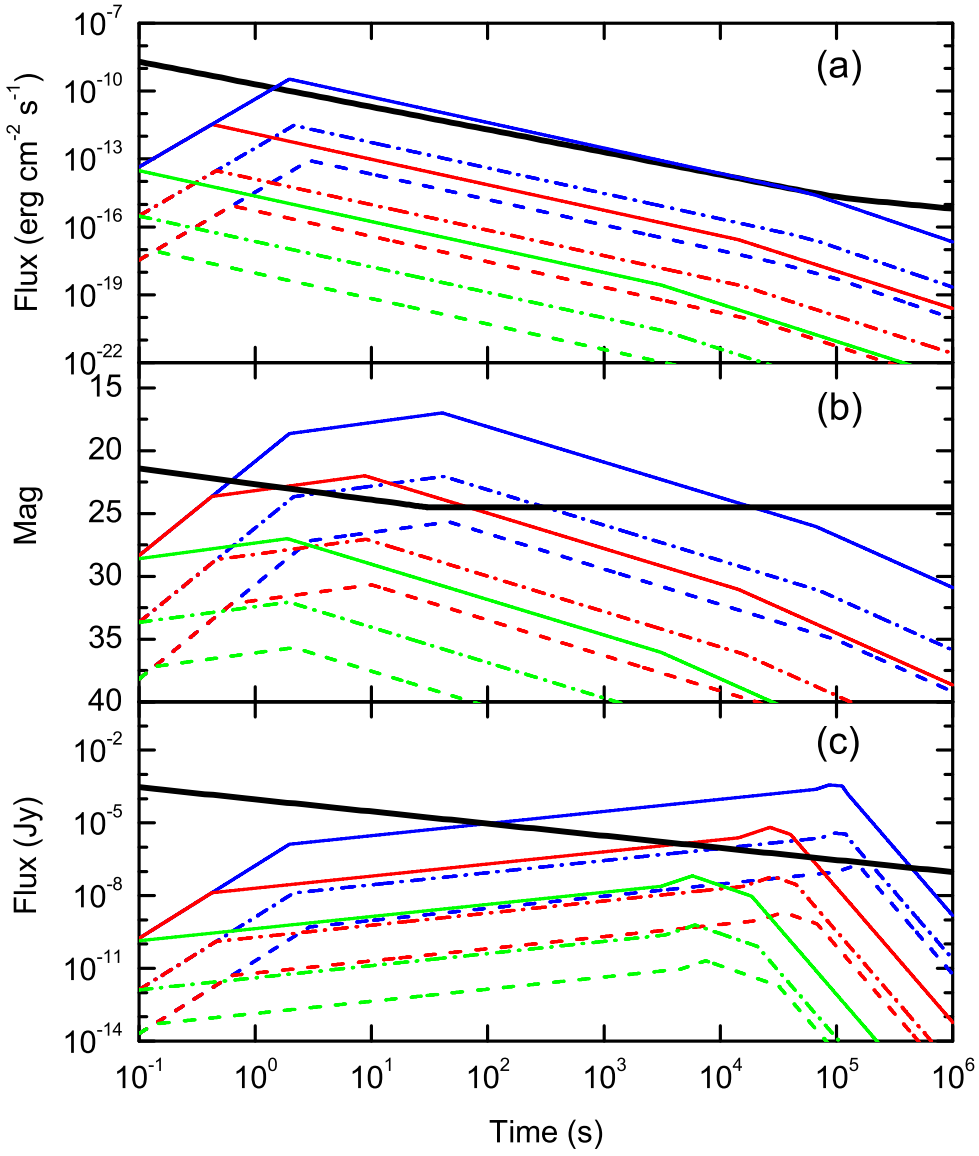

Figure 1. Example forward shock afterglow light curves of FRBs. The model parameters: $\epsilon_B = 0.01$, $\epsilon_e = 0.1$, $n_0 = 1$, $p = 2.5$, and $\eta = 100$. Three values of the energy $E = 10^{47}$ (blue), 10^{45} (red), 10^{43} (green), and three values of redshift $z = 0.5$ (dashed), 0.1 (dash-dotted), 0.01 (solid) have been adopted. (a) The X-ray light curves at 2 keV, the black solid line is the detector sensitivity line of *Swift*/XRT; (b) $R-band$ light curves, the black solid line is the detector sensitivity line of LSST; (c) radio light curves at 1 GHz, the black solid line is the detector sensitivity line of EVLA.

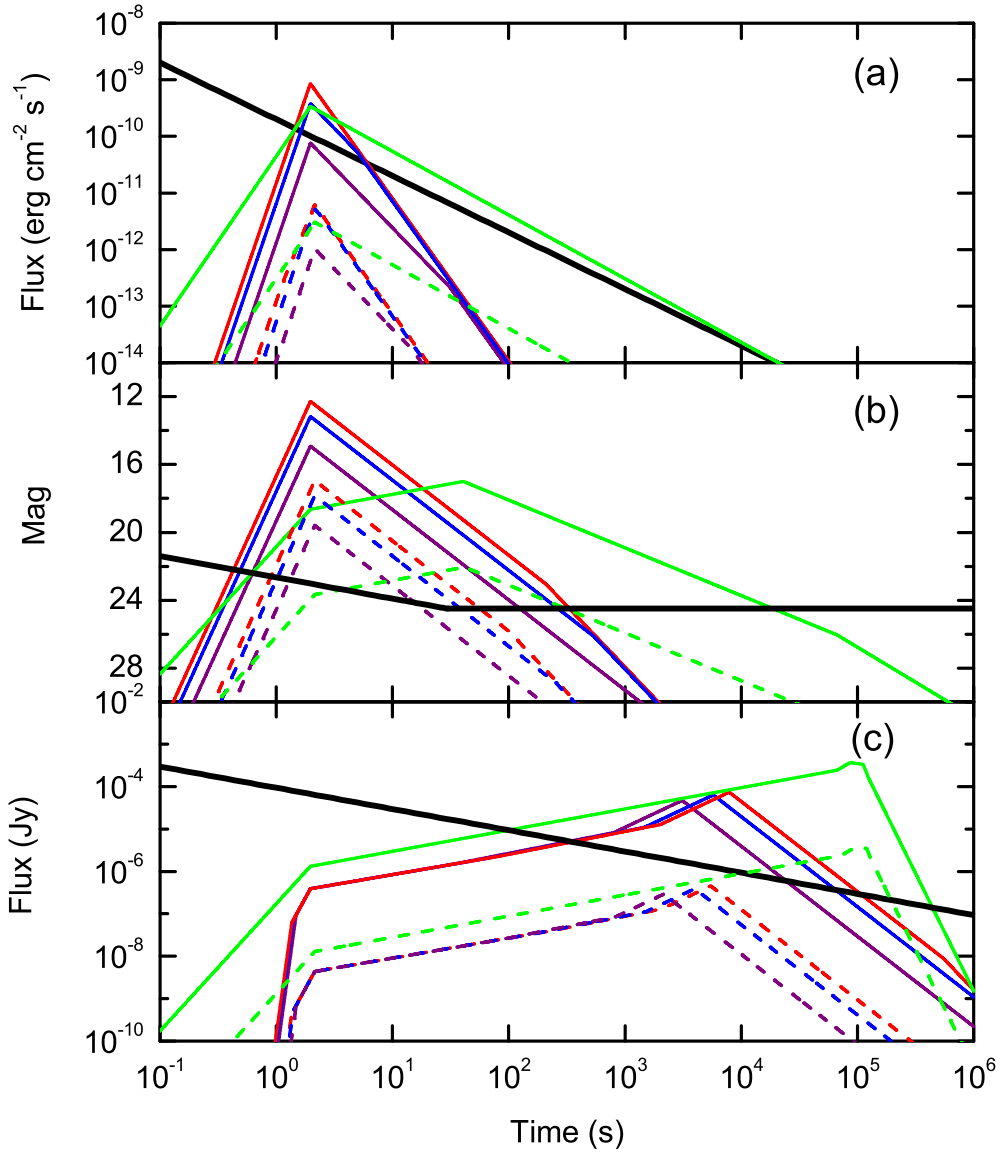

Figure 2. Example reverse shock afterglow light curves of FRBs. The model parameters: $\epsilon_e = 0.1$, $n_0 = 1$, $p = 2.5$, and $\eta = 100$. Only the most optimistic cases with energy $E = 10^{47}$ and redshift $z = 0.01$ (solid) and $z = 0.1$ (dashed) are plotted. Several $R_{\rm B}$ values are adopted to calculate the RS component: $R_{\rm B} = 2$ (purple), 5 (blue), and 8 (red). The FS component is shown as green in both cases, and the black solid lines are the detector sensitivity lines (same as Fig. 1). (a) The X-ray light curves at 2 keV; (b) $R-band$ light curves; (c) radio light curves at 1 GHz.

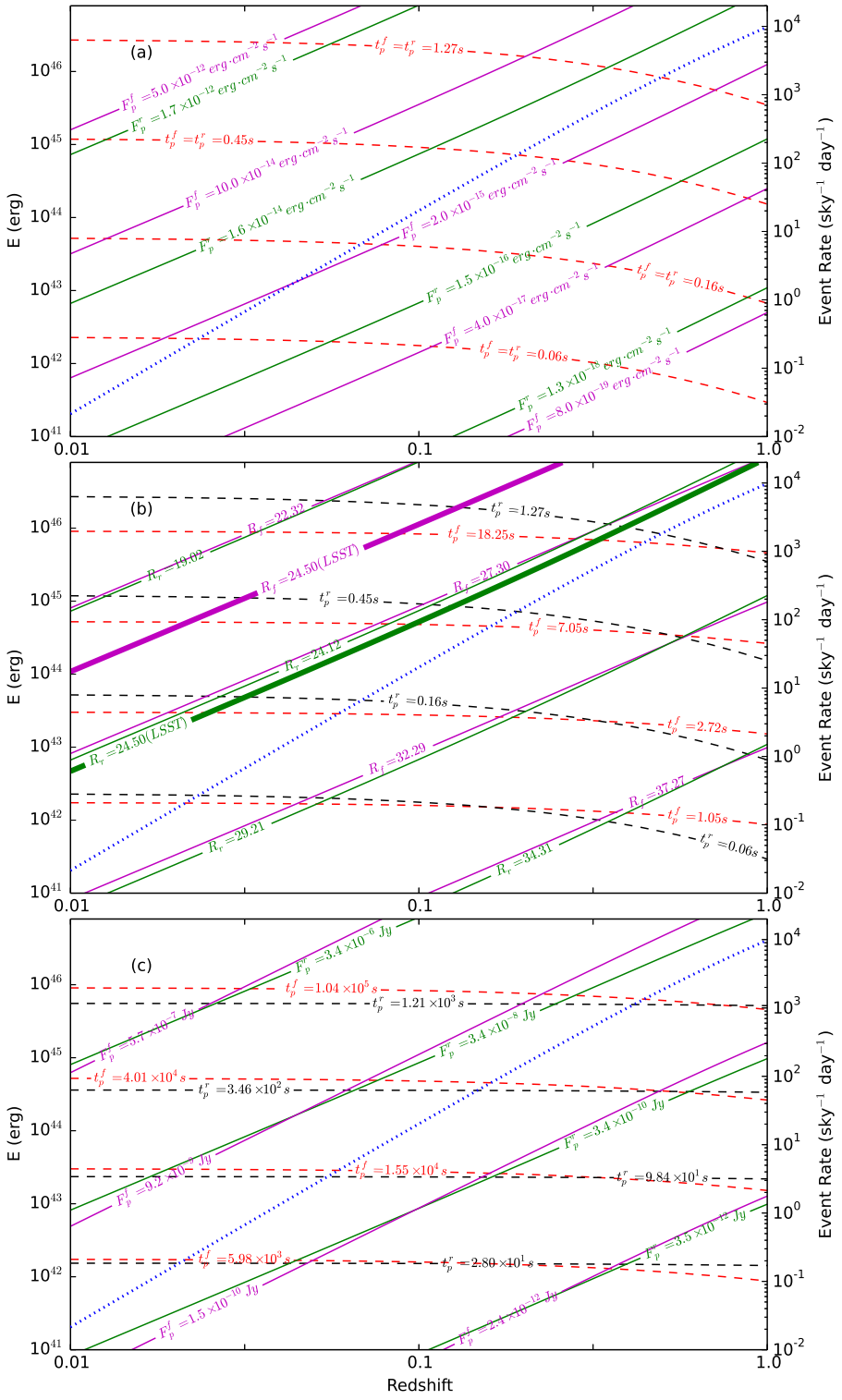

Figure 3. Contours of peak time and peak flux in the $E-z$ plane. The peak times are marked in dashed lines (the red for FS and the black for RS), and peak fluxes are marked in solid lines (the purple for FS and the green for RS). The blue dotted line in each panel denote the detection event rate (right vertical label). Panels (a), (b), and (c) are for X-rays, optical, and radio bands, respectively. Thick lines in panel b are the sensitivity lines of LSST in the survey mode: FS (magenta) and RS (green).

.